Journal of Inorganic Biochemistry 256 (2024) 112567

Contents lists available at ScienceDirect

Journal of Inorganic Biochemistry

journal homepage: www.elsevier.com/locate/jinorgbio

Unveiling the mechanism of activation of the Te(IV) prodrug AS101. New chemical insights towards a better understanding of its medicinal properties

Lorenzo Chiaverini [a], Iogann Tolbatov [b,*], Alessandro Marrone [c,*], Tiziano Marzo [a,*], Tarita Biver [d,1], Diego La Mendola [a,1]

[a] Department of Pharmacy, University of Pisa. Via Bonanno Pisano 6, 56126 Pisa, Italy
[b] Department of Physics and Astronomy, University of Padova, via F. Marzolo 8, 35131 Padova, Italy
[c] Department of Pharmacy, Università degli Studi "G. D'Annunzio" Chieti-Pescara, Via dei Vestini, 66100 Chieti, Italy
[d] Department of Chemistry and Industrial Chemistry, University of Pisa, Via G. Moruzzi, 13, 56124 Pisa, Italy

ARTICLE INFO

Keywords:
AS101
Metalloid-based drugs
Inorganic drugs
Tellurium
Prodrugs
DFT

ABSTRACT

AS101 (Ammonium trichloro (dioxoethylene-O,O′) tellurate) is an important hypervalent Te-based prodrug. Recently, we started a systematic investigation on AS101 with the aim to correlate its promising biological effects as a potent immunomodulator drug with multiple medicinal applications and its specific chemical properties. To date, a substantial agreement on the rapid conversion of the initial AS101 species into the corresponding $TeOCl_3^-$ anion does exist, and this latter species is reputed as the pharmacologically active one. However, we realized that $TeOCl_3^-$ could quickly undergo further steps of conversion in an aqueous medium, eventually producing the TeO_2 species. Using a mixed experimental and theoretical investigation approach, we characterized the conversion process leading to TeO_2 occurring both in pure water and in reference buffers at physiological-like pH. Our findings may offer a valuable "chemical tool" for a better description, interpretation -and optimization- of the mechanism of action of AS101 and Te-based compounds. This might be a starting point for improved AS101-based medicinal application.

1. Introduction

Inorganic drugs represent an essential resource in medicine for applications in both diagnosis and therapy [1–4]. The large variety of oxidation states, coordination geometries and reactive features make metals and metalloids extremely versatile and useful for the preparation of molecules capable of reacting with biological substrates, thus inducing pharmacological effects [5]. Among several examples are the worldwide approved platinum-based drugs for cancer treatment as well as the wide plethora of radioactive nuclide-bearing complexes applied in imaging techniques and for specific therapeutic applications [6–8]. In this context, as shown by the unreplaceable role of As_2O_3 (Trisenox®) in the current clinical protocols for treating acute promyelocytic leukemia (APL), metalloids may also have a relevant impact [9–11]. Recently, we started investigating tellurium-based compounds with particular attention to the hypervalent compound known as AS101. This compound was originally developed and studied by Albeck, Sredni and co-workers at Bar-IIan University, Israel, where they discovered its outstanding immunomodulatory properties [12]. Specifically, this is the only Te-based molecule that entered clinical trials against various pathological conditions, including thrombocytopenia in solid tumor patients, external genital warts, atopic dermatitis, elderly acute myeloid leukemia (AML), myelodysplastic syndrome (MDS) and other diseases (for a complete overview on the completed/ongoing clinical trials, see ClinicalTrials.gov) [13]. The pharmacological effects of AS101 mainly arise from the presence of the tellurium(IV) that has a high affinity for thiol residues; accordingly, its quick reactivity and coordination towards cysteine proteases are at the molecular basis of the immunomodulatory features [14–16]. Interestingly, some studies revealed that AS101 rapidly reacts in water media, producing the corresponding anionic oxide species $TeCl_3O^-$. This latter is reputed to be the active species, and the detailed mechanism underlying its generation from AS101 has been

* Corresponding authors.
E-mail address: tiziano.marzo@unipi.it (T. Marzo).
[1] Equally contributed

https://doi.org/10.1016/j.jinorgbio.2024.112567
Received 14 February 2024; Received in revised form 4 April 2024; Accepted 17 April 2024
Available online 19 April 2024

investigated both experimentally and computationally by us and other research groups [15,17]. Also, in the last years, some AS101 analogues and other Te(IV)-based compounds have been investigated by D'arcy, Montagner et al. with a mixed experimental-theoretical investigation. Noteworthy, in a paper published in 2019, they reported on a series of compounds of general formula $NH_4[(RC_2H_3O_2)Cl_3Te]$, (where R stands for an alkyl group with different chain length). They also tried to make a correlation between the compounds' chemical structure, the solution stability and antimicrobial properties. It was possible to straightforwardly assess that longer R chains determined higher water stability, nevertheless, this observation was enough to make a direct correlation with the observed antimicrobial activity. The authors eventually concluded that it is the prodrug nature of the studied compounds the key aspect for the biological activity. Hence, it is the production of $TeOCl_3^-$ active species that determines the observed pharmacological result [18]. Additionally, in another paper published in 2023, the same authors reported on some novel dihydroxazole Te-hexachloride salts fully characterized in their solution behavior and, preliminarily, on their anticancer properties. Interestingly, under the used experimental synthetic conditions, TeO_2 is formed as byproduct derived from the hydrolysis of $TeCl_2(OH)_2$ species [19]. However, more recently, we carried out further experiments on the AS101 activation process, realizing that $TeCl_3O^-$ can further and rapidly convert into TeO_2. Previous -but still very sporadic- reports mentioned the formation of species different from $TeCl_3O^-$ upon incubation of AS101 in the presence of water, but no detailed investigation on the process leading to their formation was done [20]. Spurred by this evidence, we focus our efforts on a more detailed description of the AS101 activation process. Indeed, the mechanistic description of the production of TeO_2 as the resulting species from AS101 may have a relevant impact on the pharmacological profile of AS101. Accordingly, we report here a study that, starting from experimental observation and thanks to a detailed theoretical analysis of the mechanism of conversion, allows us to depict a clear and more comprehensive picture of the fate that AS101 undergoes in aqueous media.

2. Results and discussion

2.1. Solution studies

AS101 is a potent immunomodulator agent whose synthesis is simple and affords the product in good yield [13,15,21,22]. The complex can be obtained by refluxing $TeCl_4$ in anhydrous MeCN in the presence of an excess of anhydrous ethylene glycol for a few hours. The white solid precipitates from the solution and can be then collected and washed with anhydrous MeCN. This procedure affords the product free of impurities. AS101, as well as its derivatives and other inorganic tellurium compounds, is highly sensitive to water and readily hydrolyses losing the coordinated ethylene glycol (Fig. 1) [15].

This process can be easily followed using ^1H and ^{13}C NMR spectroscopy, and the mechanism for the formation of the oxide species $TeOCl_3^-$ has been studied to better understand the activation mechanism of AS101 [15,17]. There is a substantial agreement concerning the rapid conversion of AS101 into the corresponding $TeOCl_3^-$ anion, which is considered to be the prevalent species forming in presence of a large excess of water, and therefore, the pharmacologically active one [17]. However, we realized how the addition of water to AS101 may lead to the formation of the TeO_2 species that precipitates (Fig. 1). We have analysed this process in pure water and calculated from the solid TeO_2 formed that this product is obtained in good yields (>60%). This finding indicates that, even if the conversion of AS101 is not quantitative, the TeO_2 oxide is the prevalent species in these conditions. The same experiment was also performed using a phosphate buffer saline (PBS) buffer solution (pH = 7.4) and cacodylate buffer solution (pH = 7) obtaining the same result. In these latter cases, the ratio between AS101 and the buffer concentration was the same as used in the subsequent spectrophotometric experiments (vide infra). TeO_2 was confirmed via IR spectroscopy and oxygen elemental analysis. In the IR spectrum, only two strong bands at 593 cm^{-1} and 730 cm^{-1} are present, which may be attributed to the vibration of the Te—O bond (Fig. S1) [23,24]. Moreover, the oxygen percentage that was found with the elemental analysis agrees with the one expected for the species TeO_2. This finding was quite surprising to us since, in the current literature, there is a substantial lack of information concerning the formation of TeO_2 as a hydrolysis product of AS101. Among the published papers dealing with AS101 behavior in water, only one mentions the formation of species other than $TeOCl_3^-$ when AS101 is treated with a large excess of water [20]. The evidence that TeO_2 forms implies that $TeOCl_3^-$ could quickly undergo further steps of conversion in water media which were thus investigated.

The addition of AS101 to water leads to an immediate drop of the pH level (3.41 for a 2.74 × 10^{-4} M solution) suggesting that the chloride ligands are quickly displaced with simultaneous release of protons (Fig. 1) upon dissolution of AS101. No further changes in the pH values were observed even after one hour from addition. The pH measurements done (see the experimental section for details) enabled us to calculate the equivalents of H^+ released upon dissolving a known amount of solid AS101: they turned out to be equal to 1.4. These findings hint that the release of the chloride ligands and H^+ is immediate and non-quantitative, which is fully consistent with the computational outcome (vide infra). A similar behavior occurs when tellurium chlorides ($TeCl_4$ and $TeCl_2$) are treated with water, forming HCl and tellurous acid H_2TeO_3 [25].

The behavior of AS101 in solution was then studied spectrophotometrically both in DMSO, sodium cacodylate (NaCac) and PBS, at physiological-like pH. NaCac is dimethylarsinic acid sodium salt; it is one of the reference buffers for bioinorganic studies with nucleic acids and in proteomics research, and it is used in particular in the case phosphate is better avoided [26]. It is more inert than others (cannot compete with DNA's phosphates), very stable with temperature but may coordinate metal or metalloid ions [27]. On this basis, we thought it would be of interest to compare the behavior of AS101 in two salt media (cacodylate and phosphate) as they may both represent species present in some protocols or in real biological samples and help enlighten the activation path of the Te(IV) prodrug by interfering with it due to some coordination.

We focused our attention on the wavelength range > 260 nm, out of any solvent cutoff and/or any strong signal due to the more energetic UV transitions. The UV–Vis absorption spectrum of AS101 in DMSO shows no band in this area (also due to a strong DMSO background), whereas freshly prepared aqueous solutions of AS101 in cacodylate, manifest a characteristic absorption peaked at 273 nm (Fig. 2A).

The band increases in intensity and is shifted towards a higher wavelength (maximum at 286 nm) if the NaCl content is increased from 0.1 to 1.0 M; on the other hand, no similar band is present in NaCl without cacodylate or in the same 0.1 M NaCl, 0.01 M NaCac mixture if temperature is raised from 25.0 to 60.0 °C (Fig. 2A). The spectrum of

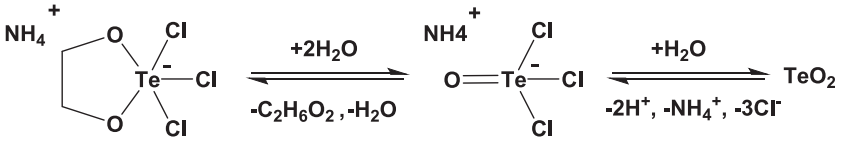

Fig. 1. Reaction scheme for the hydrolysis of AS101 with the production of TeO_2 as the final species.

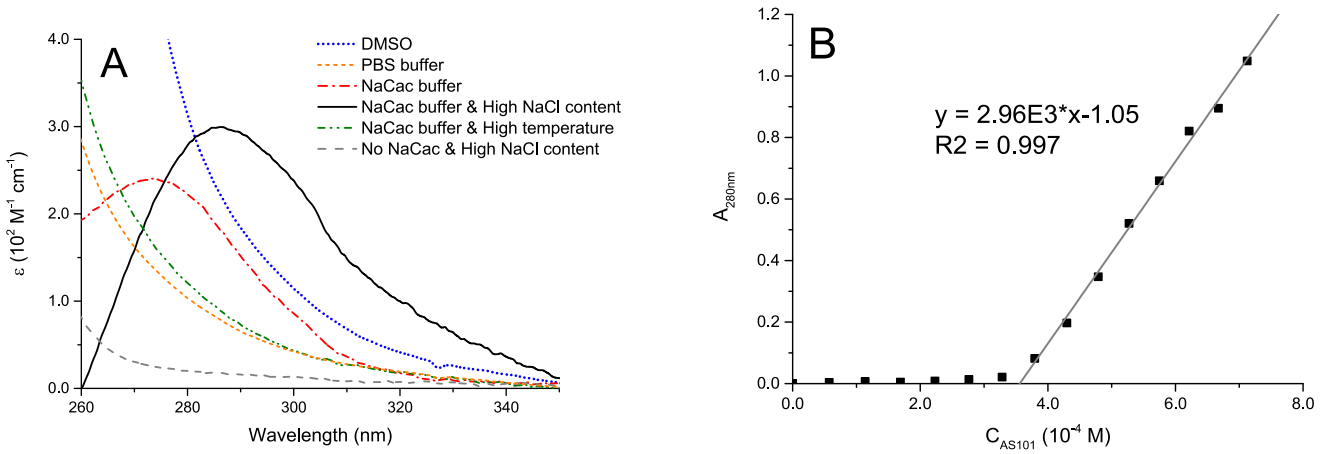

Fig. 2. (A) Absorbance profiles of AS101 in different conditions ($C_{AS101} = 5.5 \times 10^{-4}$ M; PBS = 0.01 M phosphate, 0.137 M NaCl; NaCac buffer = NaCl 0.1 M, NaCac 0.01 M, 25.0 °C; NaCac buffer & High NaCl content = NaCl 1.0 M, NaCac 0.01 M, 25.0 °C; NaCac buffer & High temperature = NaCl 0.1 M, NaCac 0.01 M, 60.0 °C; No NaCac & High NaCl Content = NaCl 1.0 M, 25.0 °C); (B) absorbance signal at 280 nm vs. AS101 concentration plot (NaCac 0.01 M).

AS101 was also acquired in PBS: despite the presence of NaCl and an AS101 concentration same as in cacodylate, no absorption at 280 nm was observed. To gain more insights into the nature of the species responsible for the absorption at ca. 280 nm, we recorded spectra at increasing concentrations of AS101 (25.0 °C). Interestingly, no significant absorbance value is recorded at the diagnostic 280 nm wavelength until a concentration threshold (3.5×10^{-4} M) is reached in the cuvette, after which a linear response of the system following Lambert-Beer's law is observed (Fig. 2B); such a broken-line plot is typical of the presence of a critical aggregation concentration [28].

Based on these findings, we started hypothesizing that the species responsible for the absorption band around 280 nm were aggregates containing tellurium-chloride bonds. The aggregate species starts forming only above a certain concentration and, according to their labile nature, are not formed at high temperatures. However, aggregation does not occur in NaCl 1.0 M only at 25.0 °C: this led us to assume that aggregation also depends, beyond the pH, on the presence of cacodylate. The effect of the pH was not surprising, as in the literature different studies concerning the aqueous speciation of $TeCl_4$ report the presence of different chlorotellurate(IV) species depending on the pH values and the chloride concentration of the solution; furthermore, some of these species absorb near 280 nm [29]. The buffer-specific response could be explained due to the well-known different modulation of the Hofmeister effects disclosed by the two salt media [30,31]. Indeed, the aggregation of species featured by Te—Cl functional groups is expected to be influenced by the lyotropic properties of the bulk, especially in the early stages of aggregation in which non-covalent interactions are dominant. On the other hand, there should be a role of phosphate or cacodylate in the AS101 speciation. We envisioned that, while cacodylate does not interfere with the formation of the species that aggregate, phosphate anion may react with either AS101 or its hydrolytic derivatives affecting the aggregation process. Accordingly, the phosphate coordination may yield a species that does not aggregate, thus explaining the lack of UV–vis absorption.

It should be also noticed that TeO_2 formation occurs in the presence of both cacodylate and phosphate, indicating that none of these species prevents the production of TeO_2 as the final product. The maximum around 280 nm, interestingly, was found to be unstable in time and fades out in the 2–3 h time range (Fig. S2).

Overall, this evidence straightforwardly confirms that, in the presence of cacodylate, the process implies the formation of transient chromophore species that over time evolves to TeO_2. Conversely, in the presence of phosphate, the mechanism for the conversion of AS101 into the TeO_2 as the final species of the hydrolytic process follows a different reaction pathway, i.e. without prior formation of aggregate species.

2.2. Theoretical calculations

Either the formation of chloro-oxo intermediates or the final TeO_2(s) product is articulated to the reaction of $TeOCl_3^-$ anion with the aqueous bulk. Hence, computational studies were first addressed to retrace the chemical events underlying the hydrolysis of $TeOCl_3^-$ and identify the most representative chemical intermediates.

The theoretical investigation of the $TeOCl_3^-$ hydrolysis was carried out at the DFT level of theory by using the pseudo-molecular approach, in which the estimate of the activation free energies for the $TeOCl_3^-$ hydrolysis steps was gained by conveniently decomposing the process as depicted in Fig. S3, using the experimental values for the vaporization free energy of water 9.72 kcal/mol [32], proton solvation free energy −265.9 kcal/mol [33], solvation free energy of chloride −74.5 kcal/mol [33].

The reactant $TeOCl_3^-$ forms the RA1 reaction adduct (−7.7 kcal/mol, Fig. 3) with the first attacking water molecule. The first transition state (TS1) leading to the release of the first chloride has a Gibbs free energy (GFE) of 14.5 kcal/mol. This is a late TS, with Te—Cl and Te-water distances being 3.30 and 2.39 Å (Fig. 4), respectively, that evolves into a product adduct PA1 with GFE of −4.1 kcal/mol, in which the protonated Cl is detached and stays nearby being weakly coordinated. The protonation of the leaving chloride in the TS structure is not surprising when the implicit solvation is employed to simulate the aqueous bulk. Hence, to correctly assess the process thermodynamics, the full dissociation of HCl(aq) was always assumed and the GFE of this species was estimated with the sum of $\Delta G^0(H^+(aq))$ and $\Delta G^0(Cl^-(aq))$ (See Experimental section, Computational Details). The attack of the second water molecule starts with the formation of RA2 adduct (−10.5 kcal/mol). The subsequent TS2 (10.1 kcal/mol) features incoming water (Te—O distance of 2.46 Å) and leaving chloride (Te—Cl distance of 3.34 Å); however, it does not result in the formation of a Te—O bond (Fig. 4). Indeed, the resulting product-adduct (6.1 kcal/mol) includes a water molecule weakly coordinated to the metal center, whereas the chloride atom protonates by one of the water hydrogens. Hence, while the first hydrolysis step is described by the concerted entering nucleophile attack/leaving group release, the second hydrolytic step resembles a S_N1-like mechanism, in which the leaving group detachment precedes the binding of the entering nucleophile. In our reaction model, the final binding of water to Te is concomitant with a barrierless water-to-chloride proton shift that yields the Int2 species (−0.2 kcal/mol), and, afterwards, eventuates in the formation of the $TeO(OH)_2Cl$ with the GFE of −0.7 kcal/mol. Again, such a proton transfer is an artifact caused by the use of implicit solvation; on the other hand, we expect that Int2 species is quite acidic and releases one proton and one chloride to the

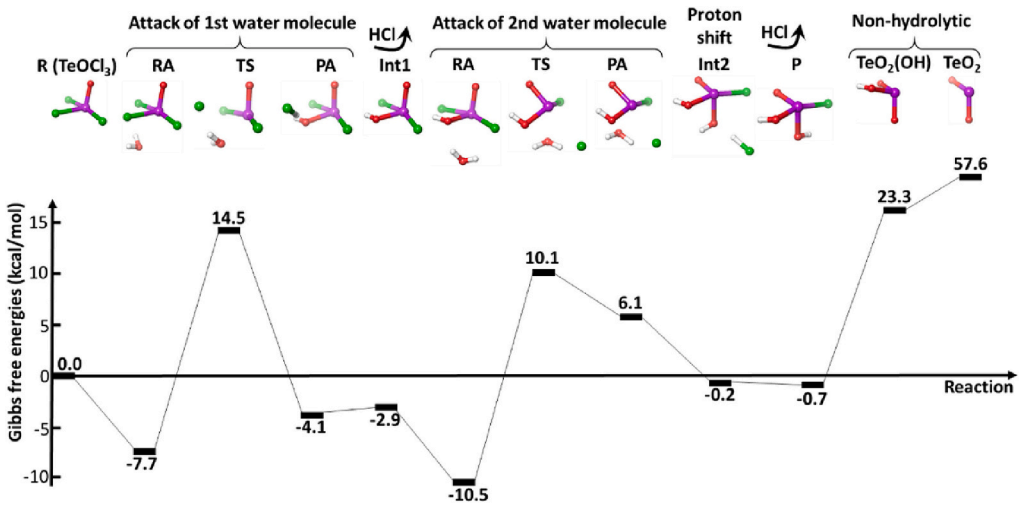

Fig. 3. Reaction mechanism for $TeOCl_3^-$ in the presence of water (top) and computed reaction profiles for the hydrolysis of $TeOCl_3^-$ (below). The last two structures do not include the hydrolytic cleavage, nevertheless, we included them for the sake of completeness. Gibbs free energy (GFE) values in kcal/mol are displayed. R, RA#, TS#, PA#, Int#, and P stand for reactant, reactant-adduct, transition state, product-adduct, intermediate, and product, respectively. Colour scheme for the 3D structures in Figs. 3–5: Te (plum), Cl (green), O (red), P (violet), As (blue), C (grey), and H (white). (For interpretation of the references to colour in this figure legend, the reader is referred to the web version of this article.)

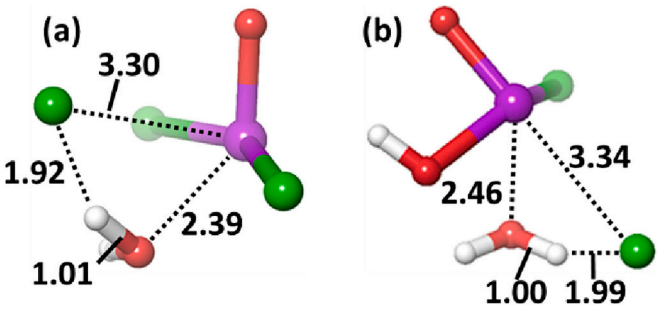

Fig. 4. Transition states corresponding to the attack of the first (a) and second (b) water molecules. Distances between atoms are shown in angstroms.

bulk to form the species.

Therefore, DFT calculations displayed that the release of the third chloride, in analogy to the second hydrolysis step, presumably occurs via a dissociative mechanism, although all attempts to optimize the corresponding transition state structure were unfruitful. The species eventually produced by the complete hydrolysis of $TeOCl_3^-$, i.e. the tellurous acid $TeO_2(OH)$ and the corresponding oxide TeO_2, were estimated at rather high energies, 23.3 and 57.6 kcal/mol, respectively. On the other hand, these species are formed with the release of three equivalents of hydrogen chloride per $TeOCl_3^-$, and, thus, are expected to rapidly and irreversibly lead to the TeO_2(s) precipitation. Above all, DFT calculations evidenced that $TeOCl_3^-$ hydrolysis is both thermodynamically and kinetically favorable, and that the first hydrolysis step is rate-determining. This process can be modelled as a pseudo-first-order reaction with an estimated barrier of 14.5 kcal/mol. Therefore, the second and third hydrolytic steps are much faster and occur via different mechanisms, characterized by the earlier solvolysis of the Te—Cl bond. The first and second hydrolysis steps were characterized by small values of the reaction free energy and thus correspond to two equilibria. The latter computational outcome is fully consistent not only with the incomplete chloride release evidenced by the experimental yields (see above) but also with the finding that chloride concentration can modulate the formation of aggregates. Indeed, high concentrations of chloride may left-shift the second and third hydrolysis steps, which eventuate into an increase of $TeO(OH)Cl_2^-$ concentration. The formation of chloro-oxo soluble species and their persistence, especially at high chloride concentrations, may eventuate in their aggregation, in agreement with the UV–Vis experiments (see above). Therefore, we envision that all hydrolytic steps, being accompanied by the release and dissociation of HCl, are all characterized by positive reaction entropy values. In this line, we hypothesize that all hydrolytic steps are thermodynamically favored by increasing temperature, thus, the lack of chloro-oxo species aggregation, experimentally detected at 60 °C, could be easily explained by the right-shift of all hydrolytic steps, and the consequent decrease of the concentration of these intermediate species.

Based on the significant concentration of buffer ions, these species may compete with water in the reaction with $TeOCl_3^-$. Indeed, both cacodylate and phosphate anions can coordinate at the Te center by yielding either mono or bidentate adducts. In the latter case, a chelate effect may occur by favouring the formation of buffer-chelate over hydrolysis species.

To assess the possible involvement of phosphate or cacodylate in the chemical modulation of the AS101 speciation, the thermodynamics of the reaction between $TeOCl_3^-$ and either $H_2PO_4^-$ or $(CH_3)_2AsO_2^-$ anions were computationally assessed. We assumed that both species anions afforded the chelation of the Te center, and the concomitant release of two chloride ions could provide for a consistent and favorable entropy contribution to the process. Indeed, the substitution of one chloride by either dihydrogenphosphate or cacodylate anion was found to be exergonic by −3.9 or − 13.4 kcal/mol, respectively (Fig. 5).

Surprisingly, our calculations unveiled that while the formation of the chelate species, A, by the release of the second chloride from the $[(H_2PO_4)TeOCl_2]^-$ species, was highly endergodic +13.0 kcal/mol, the reaction with cacodylate was affected by a lower endergodicity, i.e. +4.4 kcal/mol, and, more importantly, yielded the monodentate species, B (Fig. 5, top). Hence, the overall substitution of two chloride ions by either $H_2PO_4^-$ or $(CH_3)_2AsO_2^-$ anion resulted to be endergodic (+9.1 kcal/mol) and exergodic (−9.4 kcal/mol), respectively (Fig. 5, top). Such a different chemical response could explain why the aggregation of chloro-oxo Te species occurs in cacodylate but not in phosphate. Indeed, we envision that the aggregation of the TeOCl moieties in B could be favored by the low coordination number of Te center, facilitating their coordinative assembly (Fig. 5, bottom). On the other hand, the formation of a species with a low coordination number of Te starting from $TeOCl_3^-$ and phosphate was found to be thermodynamically unfavourable. Moreover, even in case a small amount of phosphate adducts is formed, the resulting TeOCl moieties would be featured by a higher

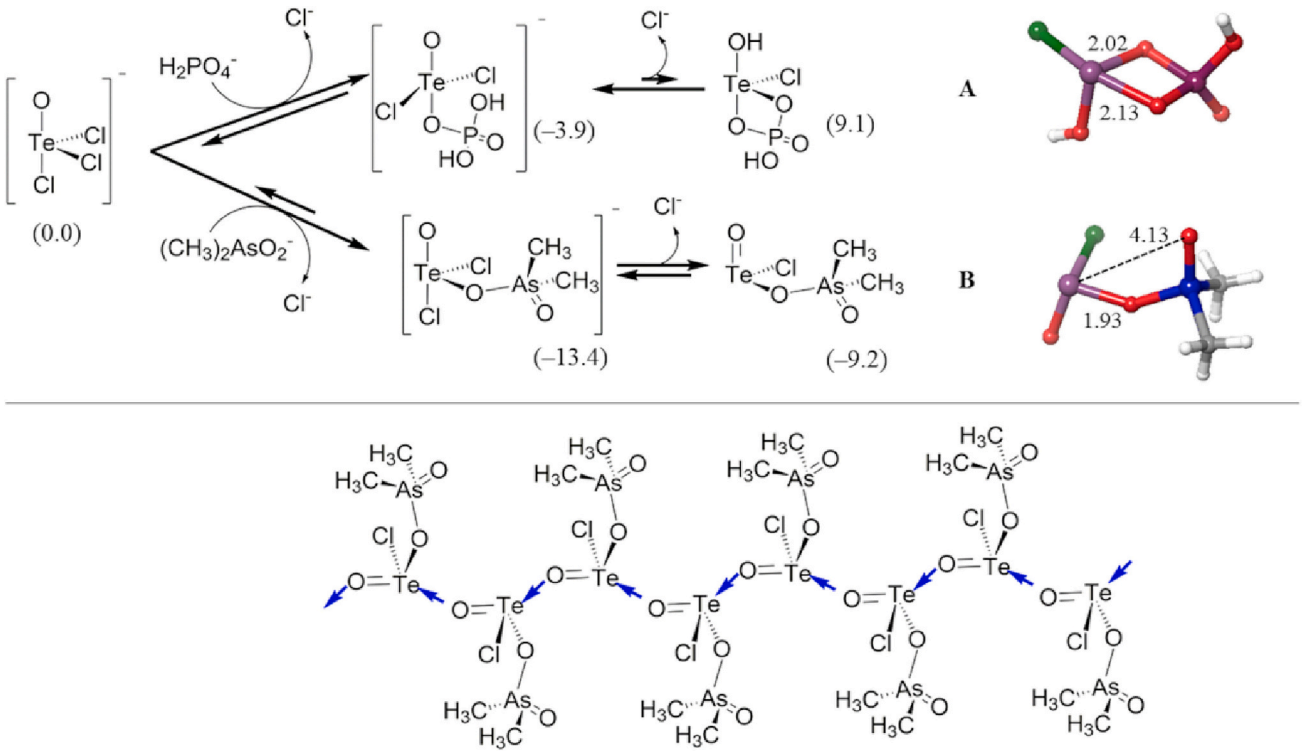

Fig. 5. Top: The release of chloride from $TeOCl_3^-$ by the reaction with buffer species, $H_2PO_4^-$ or $(CH_3)_2AsO_2^-$, yielding the chelate complex A or the monodentate complex B, respectively, and their respective ball-and-stick renditions (bond distances in angstroms). The calculated free energies relative to reactant species are reported (values in kcal/mol). Bottom: rendition of the coordinative assembly of species B. The interunit coordinative interactions are indicated by blue arrows. (For interpretation of the references to colour in this figure legend, the reader is referred to the web version of this article.)

coordination number, which would limit the assembly capability of this Te species. Therefore, the presence of acidic groups in the phosphate adduct suggests that, once formed, these species may acquire a negative charge by deprotonation, thus, resulting in being even less prone to aggregation. To corroborate our hypothesis, the pKa values of the cacodylate or phosphate adducts were calculated by employing an elsewhere reported approach [34].

As shown in Table 1, the protonation of species B is unfavourable so this monodentate, neutral species is prevalent when cacodylate is present. On the other hand, the bidentate species A, presumably formed in phosphate, resulted to be a strong acid (estimate pKa = −1.1) thus promptly yielding the corresponding anionic form $[(HPO_4)TeCl(O)]^-$ (Table 1).

The DFT investigation provided a clearer insight into the chemical processes and their articulation when the hydrolysis of AS101 occurred in either phosphate or cacodylate. The high stability of the $TeO(OH)Cl_2^-$ intermediate suggests that this species can be formed at high amounts, consistently with the formation of aggregates bearing the Te—Cl bond in their structure. The different response of the AS101 hydrolysis to the salt medium was also interpreted in the light of our DFT studies. Indeed, the reaction of $TeOCl_3^-$ with $H_2PO_4^-$ anion was calculated to be rather endergodic so we expect that this species did not or only marginally affect the hydrolysis process and the eventual formation of TeO_2 precipitate. Therefore, calculations showed that complex A, resulting from the reaction of $TeOCl_3^-$ with $H_2PO_4^-$, could hardly aggregate because: i) it would be formed in relatively low amounts, ii) the bidentate coordination of phosphate limits the coordinative assembly of Te-scaffolds, iii) once formed, this species deprotonates (low pKa) yielding a charged species whose aggregation is electrostatically hampered. On the other hand, the reaction of $TeOCl_3^-$ with cacodylate yields the neutral and monodentate species B in which the TeOCl scaffold bears a coordination vacancy on the Te center that favors its coordinative assembly. Although the participation of the uncoordinated As═O bond in the complex B assembly cannot be ruled out, the proposed aggregation model (Fig. 5, bottom) can be more easily intercepted along the overall AS101 hydrolysis eventuating in the TeO_2(s) precipitation. Indeed, we envision that the TeOCl aggregates formed in the presence of cacodylate may easily yield TeO_2 aggregates by the downstream hydrolysis of Te—Cl and Te–cacodylate coordinative bonds. An overall sketch resuming the possible AS101 activation processes emerging from the present experimental/theoretical investigation is provided in Fig. 6.

Table 1
Experimental versus estimate pKa values. Species A and B (Fig. 5) are indicated.

Acid	Base	pKa (exp)	pKa (est)
H_3PO_4	$H_2PO_4^-$	2.0	1.4
$H_2PO_4^-$	HPO_4^{2-}	6.8	6.4
HPO_4^{2-}	PO_4^{3-}	12.5	12.1
$TeO(OH)_2$	$TeO_2(OH)^-$	2.7	3.5
$TeO_2(OH)^-$	TeO_3^{2-}	8.0	8.6
TeOCl(OH)	TeO_2Cl^-	n/a	1.8
$[(CH_3)_2AsO_2TeCl(OH)]^+$	$(CH_3)_2AsO_2TeOCl$ (B)	n/a	−2.0
$(HPO_4)TeCl(OH)$ (A)	$[(HPO_4)TeCl(O)]^-$	n/a	−1.1
$(HPO_4)TeCl(OH)$ (A)	$[(PO_4)TeCl(OH)]^-$	n/a	0.2
$[(H_2PO_4)TeCl(OH)]^+$	$(HPO_4)TeCl(OH)$	n/a	−3.7

2.3. Experimental section

All solvents and reagents were purchased from Sigma-Aldrich and used without further purification. The studied compounds were stored in a dryer over $CaCl_2$. The phosphate buffer saline (PBS) solution at pH 7.4 for spectrophotometric studies was prepared by dissolving a PBS tablet in 200 mL of deionized water (0.01 M phosphate, 0.0027 M KCl and 0.137 M NaCl). The cacodylate buffer solution at pH 7.0 was freshly prepared by weight with a final composition of 0.1 M NaCl +0.01 M sodium cacodylate (NaCac). The pH measurements were made using an XS pH 7 Vio pH-meter equipped with an Ag/AgCl electrode. Elemental

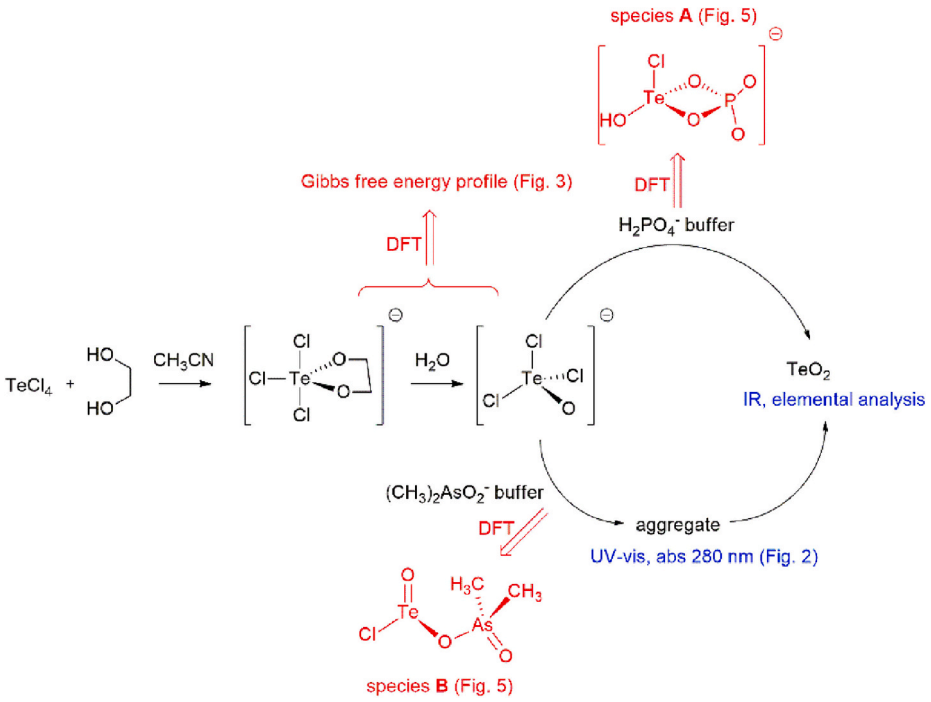

Fig. 6. The overall AS101 activation scenario. The theoretical and experimental results corroborating the crucial stages of the process yielding the formation of the TeO_2 were reported in red and blue, respectively. (For interpretation of the references to colour in this figure legend, the reader is referred to the web version of this article.)

analysis (carbon, hydrogen, nitrogen, and oxygen) was accomplished through the VarioMICRO elemental analyser. The IR spectra were recorded with an Agilent Cary 660 FTIR Spectrometer. IR spectra were processed with Spectragryph software. The UV–Vis spectra were recorded on a Shimadzu (Kyoto, Japan) 2450 UV–vis spectrophotometer, thermostated at 298.2 K (thermoelectric Peltier element with ±0.1 K accuracy) using quartz cuvettes (o.p. 10 mm). The UV–Vis spectra were processed with Origin 8.5 software. Corrections for scattering on the UV–Vis spectra were made according to the procedure described by Leach and Sheraga [35].

2.3.1. *Preparation of AS101 and conversion to TeO_2*

The synthesis of AS101 was carried out according to the reported procedures [15]. Briefly, the reaction mechanism involves two molecules of ethylene glycol: one coordinates to the tellurium center while the other, after being halogenated, reacts with acetonitrile leading to the eventual formation of NH_4Cl and 2-chloroehtyl acetate as a byproduct [13]. Elemental Analysis (CHN): $C_2H_8Cl_3NO_2Te$ requires: C, 7.70; H, 2.58; N, 4.49; Found: C, 7.66; H, 2.37; N, 4.50. ^1H NMR (400 MHz; DMSO-d [6]): 7.22 (4H; NH_4^+); 4.38 (s; 4H; CH_2).

The conversion of AS101 into TeO_2 was obtained by using the following procedure. To a small quantity of AS101 (114 mg; 0.37 mmol), 5 mL of HPLC grade water were added in a 10 mL round bottom flask. The suspension was magnetically stirred for two hours; after this time, the colourless solid was separated by decantation, washed with water, methanol and dried under vacuum over $CaCl_2$. Yield: 57%. Elemental Analysis (%O): TeO_2 Requires: 20.05. Found: 20.40 IR (cm^{-1}): 729.9 s (ν Te—O); 593.1 s (ν Te—O), see supporting material for IR spectrum, Fig. S1.

The same procedure was used for obtaining TeO_2 from a PBS buffer solution or cacodylate buffer solution, maintaining the ratio between the concentration of drug and the buffer the same as in the spectrophotometric experiments. Yield: 63%.

2.3.2. *UV–Vis Absorption experiments*

The stock solutions of AS101 (4–6 mM) were obtained by dissolving 1–2 mg of the solid (4–6 mmol) in 1.0 mL of anhydrous DMSO. As a general procedure, 100 μL of the stock were added to a quartz cuvette containing either 1.0 mL of the sodium cacodylate buffer solution (0.1 M NaCl, 0.01 mM NaCac, pH 7.0) or the PBS buffer (0.01 M phosphate, 0.0027 M KCl, 0.137 M NaCl, pH 7.4). Other salt contents have been envisaged as detailed in the text. The resulting concentration of AS101 in the cuvette was in the 4–6 $\times$ 10^{-4} M range.

In the kinetic studies, the absorbance value at 280 nm of AS101 4.3 $\times$ 10^{-4} M was monitored over time. This experiment was done in triplicate. For the experiments at different AS101 concentration, 10 μL of a 5.8 $\times$ 10^{-3} M stock solution of AS101 in anhydrous DMSO were gradually added to a cacodylate buffer solution directly in the spectrophotometric cell until a concentration of 7.1 $\times$ 10^{-4} M was reached. A spectrum was recorded after each addition. The spectra were quickly acquired and at constant time intervals to minimize the effect of the diminishing of the absorbance at 280 nm due to the conversion to TeO_2.

2.3.3. *pH measurements*

A stock solution of AS101 4.7 $\times$ 10^{-1} M was prepared by dissolving 14.8 mg (0.047 mmol) of the compound in 100 μL of anhydrous DMSO. Next, 10 μL of the stock were added to 17.1 mL of Milli-Q water that was previously de-gassed with nitrogen for 15 min, resulting in a concentration of AS101 2.7 $\times$ 10^{-4} M. The determination of the pH value was made after magnetically stirring the solution for several minutes. This procedure was done in triplicate. The final pH measured was 3.41 for each experiment.

2.3.4. *Computational details*

The Gaussian 16 quantum chemistry package was employed for all computations [36]. All geometry optimizations were performed by using the hybrid functional ωB97X [37] with the basis set def2SVP [38,39], and by using implicit solvation to model the aqueous bulk. Frequency computations were performed at the same level of theory to verify the stationary nature of the minima and the transition states, as well as produce the zero-point energy (ZPE), vibrational corrections to thermodynamic properties, and reference state corrections [40] for liquid

phase at 1 M and 298.15 K. Intrinsic reaction coordinate (IRC) computations were utilized to determine the reagent-adduct (RA) and product-adduct (PA) minima linked to the transition states for each studied reaction step. Indeed, DFT is a ubiquitous tool in bioinorganic chemistry [41–43] that allows accurate characterization of the structures and reaction pathways for the complexes with transition metals [44–46]. The density functional ωB97X is reputed to yield good geometrical structures and to precisely estimate the electronic energies [47–49].

The IEFPCM formalism was employed to account for solvation in water [50]. This method is known to yield free energies with considerably smaller errors than continuum models, both for neutral and charged complexes, as recently demonstrated [51]. The solvation energies were calculated with the ωB97X / def2TZVP [38,39] method. The free energy profile for the complete $TeOCl_3^-$ hydrolysis was retraced using the thermodynamic cycle reported in Scheme S3 (see supporting material).

The electronic energies were calculated with ωB97X-D [52] / def2TZVP method, which emerged in the benchmarking (Table S1) as an accurate method reproducing well (16.4 kcal/mol) the first reaction barrier of 17.19 kcal/mol obtained from the experimental UV–Vis data (vide infra). Indeed, Table S1 reports the benchmarking of various density functionals (ωB97X-D, ωB97X, M062X [53], PBEPBE [54], BP86 [55,56], BPW91 [55,57], as well as the functionals M06L [58] and PBEPBE including Grimme's correction D3 [59]) and solvation methods (CPCM [60], SMD [61]) versus the first barrier of the studied hydrolytic degradation. The ωB97X-D yields an accurate barrier, yet it is not an outlier of the studied set, the latter corroborating its veracity. We also should note that the alteration of the solvation method affects the calculated barrier value only marginally (<1.5 kcal/mol).

To correctly account for the complete ionization of hydrogen chloride in water yielded in the investigated processes (vide infra), the Gibbs free energy of the HCl(aq) species was calculated as it follows: $\Delta G^0(\mathrm{HCl(aq)}) = \Delta G^0(\mathrm{H^+(aq)}) + \Delta G^0(\mathrm{Cl^-(aq)})$.

In which: $\Delta G^0(\mathrm{H^+(aq)}) \cong \Delta G^0_{solv}(\mathrm{H^+})$, $\Delta G^0(\mathrm{Cl^-(aq)}) = \Delta G^0(\mathrm{Cl^-(gas)}) + \Delta G^0_{solv}(\mathrm{Cl^-})$

and the solvation free energies of H^+ and Cl^- in water, −265.9 and −74.5 kcal/mol, respectively, were taken from ref. 33.

The estimate of pKa values was performed by employing an elsewhere-reported approach [34]. Briefly, the free energy for the proton exchange between any acidic species and the cacodylate anion, assumed as a reference base, was calculated at the CPCM / B3LYP [62,63] / def2TZVPP [38,39] / CPCM / B3LYP / LANL2DZ [64] level of theory. The free energy for the acidic ionization of each species was then obtained by summing up the proton exchange energy and the deprotonation free energy of the reference species. The obtained values of acidic ionization free energy (ΔG^0_{ion}) are directly related to the pKa: $\Delta G^0_{ion} = 2.3RTpKa^{theo}$. The values of pKa^{theo} for the training set species, i.e. H_3PO_4, $H_2PO_4^-$, HPO_4^{2-}, H_2TeO_3, and $HTeO_3^-$, were then regressed against the corresponding experimental pKa values to obtain a model equation (Fig. S4) for estimating the pKa of the other species.

3. Conclusions

Through the use of a combined experimental and theoretical procedure, we have carried out a study aiming to better describe the complex solution behavior of the Te(IV)-based medicinal compound AS101. Noticeably, we discover that AS101 in aqueous medium may undergo transformation finally leading to the TeO_2 species. This process occurs at physiological-like conditions, thus, it may impact the pharmacological effects of AS101. Accordingly, our findings expand the knowledge of the mechanism of activation and the chemical profile of AS101. Indeed, the current literature limits the interpretation of the promising medicinal properties of AS101, based on the rapid conversion into $TeOCl_3^-$ anion, being this latter capable of binding thiol-bearing proteins and triggering the medicinal effects [15,17]. However, this paradigm seems surmountable and limiting in the light of our findings. Hence, it hides and overlooks several important aspects concerning the solution chemistry of AS101. Thus, this manuscript starts to fill a gap in the understanding of the solution chemistry of AS101 and hopefully will contribute towards the optimization of the current AS101 medicinal application that might be the starting point for improved AS101-based treatments.

Finally, our findings might also have a practical effect because, in the preclinical as well as clinical trials, AS101 is administered in aqueous physiological solutions such as saline and phosphate-buffered saline (PBS) [17]. In this context, the formation of TeO_2 may have a practical impact being this species already been reported as biologically active [65].

Author contributions

All the authors have contributed approving the final version of the manuscript.

CRediT authorship contribution statement

Lorenzo Chiaverini: Investigation. **Iogann Tolbatov:** Writing – review & editing, Resources, Investigation. **Alessandro Marrone:** Writing – review & editing, Writing – original draft, Investigation. **Tiziano Marzo:** Writing – review & editing, Writing – original draft, Investigation, Funding acquisition, Conceptualization. **Tarita Biver:** Writing – review & editing, Investigation, Funding acquisition, Formal analysis, Data curation. **Diego La Mendola:** Writing – review & editing, Investigation, Funding acquisition.

Declaration of competing interest

There are no conflicts to declare.

Data availability

Data will be made available on request.

Acknowledgements

TM, TB, and DLM thank the University of Pisa for the financial support under the Rating Ateneo funding program. TM thanks the financial support from Ministero Italiano dell'Università e della Ricerca under the program PRIN 2022 - Progetti di Rilevante Interesse Nazionale, project code: 2022ALJRPL “Biocompatible nanostructures for the chemotherapy treatment of prostate cancer”. IT gratefully acknowledges the usage of HPC resources from Direction du Numérique – Centre de Calcul de l'Université de Bourgogne (DNUM CCUB). This work has been funded by the European Union - Next-Generation EU (“PNRR M4C2-Investimento 1.4- CN00000041”). We acknowledge the CINECA award under the ISCRA initiative, for the availability of high performance computing resources and support.

Appendix A. Supplementary data

Supplementary data to this article can be found online at https://doi.org/10.1016/j.jinorgbio.2024.112567.

References

[1] E.J. Anthony, E.M. Bolitho, H.E. Bridgewater, O.W. Carter, J.M. Donnelly, C. Imberti, E.C. Lant, F. Lermyte, R.J. Needham, M. Palau, P.J. Sadler, Metallodrugs are unique: opportunities and challenges of discovery and development, Chem. Sci. 11 (48) (2020) 12888–12917, https://doi.org/10.1039/D0SC04082G.

[2] C.J. Timothy, S. Kogularamanan, J.L. Stephen, The next generation of platinum drugs: targeted Pt (II) agents, nanoparticle delivery, and Pt (IV) prodrugs timothy,

Chem. Rev. 116 (2016) 3436–3486, https://doi.org/10.1021/acs.chemrev.5b00597.
[3] E. Alessio, Z. Guo, Metal anticancer complexes–activity, mechanism of action, future perspectives, Eur. J. Inorg. Chem. 2017 (12) (2017) 1539–1540, https://doi.org/10.1002/ejic.201600986.
[4] N. Nayeem, M. Contel, Exploring the potential of metallodrugs as chemotherapeutics for triple negative breast cancer, Chemistry– European Journal 27 (35) (2021) 8891–8917, https://doi.org/10.1002/chem.202100438.
[5] N.P. Barry, P.J. Sadler, Exploration of the medical periodic table: towards new targets, Chem. Commun. 49 (45) (2013) 5106–5131, https://doi.org/10.1039/c3cc41143e.
[6] K.A. Strohfeldt, Radioactive Compounds and their Clinical Application, Essentials Inorganic Chemistry, 2015, pp. 223–248, https://doi.org/10.1002/9781118695425.ch10.
[7] D. Cirri, L. Chiaverini, A. Pratesi, T. Marzo, Is the next cisplatin already in our laboratory? Comments Inorg. Chem. (2022) 1–14, https://doi.org/10.1080/02603594.2022.2152016.
[8] E. Boros, A.B. Packard, Radioactive transition metals for imaging and therapy, Chem. Rev. 119 (2) (2018) 870–901, https://doi.org/10.1021/acs.chemrev.8b00281.
[9] J.M. Byun, D.S. Lee, C.N. Landen, D.H. Kim, Y.N. Kim, K.B. Lee, M.S. Sung, S. G. Park, D.H. Jeong, Arsenic trioxide and tetraarsenic oxide induce cytotoxicity and have a synergistic effect with cisplatin in paclitaxel-resistant ovarian cancer cells, Acta Oncol. 58 (11) (2019) 1594–1602, https://doi.org/10.1080/0284186X.2019.1630750.
[10] T. Marzo, D. La Mendola, Strike a balance: between metals and non-metals, metalloids as a source of anti-infective agents, Inorganics 9 (6) (2021) 46, https://doi.org/10.3390/inorganics9060046.
[11] S. Shen, X.F. Li, W.R. Cullen, M. Weinfeld, X. Chris Le, Arsenic binding to proteins, Chem. Rev. 113 (2013) 7769–7792, https://doi.org/10.1021/cr300015c.
[12] B. Sredni, R.R. Caspi, A. Klein, Y. Kalechman, Y. Danziger, M. BenYa'akov, T. Tamari, F. Shalit, M. Albeck, A new immunomodulating compound (AS-101) with potential therapeutic application, Nature 330 (6144) (1987) 173–176, https://doi.org/10.1038/330173a0.
[13] L. Chiaverini, T. Marzo, D. La Mendola, AS101: an overview on a leading tellurium-based prodrug, Inorg. Chim. Acta 540 (2022) 121048, https://doi.org/10.1016/j.ica.2022.121048.
[14] A. Layani-Bazar, I. Skornick, A. Berrebi, M.H. Pauker, E. Noy, A. Silberman, M. Albeck, D.L. Longo, Y. Kalechman, B. Sredni, Redox modulation of adjacent thiols in VLA-4 by AS101 converts myeloid leukemia cells from a drug-resistant to drug-sensitive state, Cancer Res. 74 (11) (2014) 3092–3103, https://doi.org/10.1158/0008-5472.CAN-13-2159.
[15] L. Chiaverini, D. Cirri, I. Tolbatov, F. Corsi, I. Piano, A. Marrone, A. Pratesi, T. Marzo, D. La Mendola, Medicinal hypervalent tellurium prodrugs bearing different ligands: a comparative study of the chemical profiles of AS101 and its halido replaced analogues, Int. J. Mol. Sci. 23 (14) (2022) 7505, https://doi.org/10.3390/ijms23147505.
[16] D. Ling, B. Liu, S. Jawad, I.A. Thompson, C.N. Nagineni, J. Dailey, J. Chien, B. Sredni, R.B. Nussenblatt, The tellurium redox immunomodulating compound AS101 inhibits IL-1β-activated inflammation in the human retinal pigment epithelium, Br. J. Ophthalmol. 97 (7) (2013) 934–938, https://doi.org/10.1136/bjophthalmol-2012-301962.
[17] A. Silberman, M. Albeck, B. Sredni, A. Albeck, Ligand-substitution reactions of the tellurium compound AS-101 in physiological aqueous and alcoholic solutions, Inorg. Chem. 55 (21) (2016) 10847–10850, https://doi.org/10.1021/acs.inorgchem.6b02138.
[18] K. D'Arcy, A.P. Doyle, K. Kavanagh, L. Ronconi, B. Fresch, D. Montagner, Stability of antibacterial Te (IV) compounds: a combined experimental and computational study, J. Inorg. Biochem. 198 (2019) 110719, https://doi.org/10.1016/j.jinorgbio.2019.110719.
[19] K. D'Arcy, T. Schäfer, M. De Franco, R. Ricco, V. Gandin, P.J.S. Miguel, D. Montagner, Unusual tellurium (IV) mediated cyclisation diols into dihydroxazoles with potential anticancer activity, New J. Chem. 47 (39) (2023) 18485–18491, https://doi.org/10.1039/D3NJ03186A.
[20] C.R. Princival, M.V. Archilha, A.A. Dos Santos, M.P. Franco, A.A. Braga, A. F. Rodrigues-Oliveira, T.C. Correra, R.L. Cunha, J.V. Comasseto, Stability study of hypervalent tellurium compounds in aqueous solutions, ACS Omega 2 (8) (2017) 4431–4439, https://doi.org/10.1021/acsomega.7b00628.
[21] G. Halpert, B. Sredni, The effect of the novel tellurium compound AS101 on autoimmune diseases, Autoimmun. Rev. 13 (12) (2014) 1230–1235, https://doi.org/10.1016/j.autrev.2014.08.003.
[22] T.Y. Yang, S.P. Tseng, H.N. Dlamini, P.L. Lu, L. Lin, L.C. Wang, W.C. Hung, In vitro and in vivo activity of AS101 against carbapenem-resistant Acinetobacter baumannii, Pharmaceuticals 14 (8) (2021) 823, https://doi.org/10.3390/ph14080823.
[23] B. Qin, Y. Bai, Y. Zhou, J. Liu, X. Xie, W. Zheng, Structure and characterization of TeO2 nanoparticles prepared in acid medium, Mater. Lett. 63 (22) (2009) 1949–1951, https://doi.org/10.1016/j.matlet.2009.06.018.
[24] A. Amari, M.K. Al Mesfer, N.S. Alsaiari, M. Danish, A.M. Alshahrani, M.A. Tahoon, F.B. Rebah, Electrochemical and optical properties of tellurium dioxide (TeO2) nanoparticles, Int. J. Electrochem. Sci. 16 (2) (2021) 210235, https://doi.org/10.20964/2021.02.13.
[25] J.E. House, K.A. House, Descriptive Inorganic Chemistry, Academic Press, 2015.
[26] S. Brudar, B. Hribar-Lee, Effect of buffer on protein stability in aqueous solutions: a simple protein aggregation model, J. Phys. Chem. B. 125 (10) (2021) 2504–2512, https://doi.org/10.1021/acs.jpcb.0c10339.
[27] M. Lari, H.J. Lozano, N. Busto, T. Biver, J.M. Leal, S. Ibeas, J.A. Platts, F. Secco, B. Garcia, Stabilization of Al (III) solutions by complexation with cacodylic acid: speciation and binding features, Phys. Chem. Chem. Phys. 17 (44) (2015) 29803–29813, https://doi.org/10.1039/C5CP04717J.
[28] S. Liu, Y. Yang, T. Liu, The aggregation behaviors of organic radicals in polar fluorinated arenes, Aggregate (2024) e543, https://doi.org/10.1002/agt2.543.
[29] J. Milne, M. Mahadevan, Chlorotellurate (IV) equilibria in aqueous hydrochloric acid, Inorg. Chem. 23 (3) (1984) 268–271, https://doi.org/10.1021/ic00171a003.
[30] K.P. Gregory, G.R. Elliott, H. Robertson, A. Kumar, E.J. Wanless, G.B. Webber, V. S. Craig, G.G. Andersson, A.J. Page, Understanding specific ion effects and the Hofmeister series, Phys. Chem. Chem. Phys. 24 (21) (2022) 12682–12718, https://doi.org/10.1039/d2cp00847e.
[31] B.W. Ninham, P.L. Nostro, Molecular forces and self-assembly: in colloid, nano sciences and biology, Cambridge University Press, 2010, https://doi.org/10.1039/c4cs00144c.
[32] F.M. Brethomé, N.J. Williams, C.A. Seipp, M.K. Kidder, R. Custelcean, Direct air capture of CO2 via aqueous-phase absorption and crystalline-phase release using concentrated solar power, Nat. Energy 3 (7) (2018) 553–559, https://doi.org/10.1038/s41560-018-0150-z.
[33] C.P. Kelly, C.J. Cramer, D.G. Truhlar, Aqueous solvation free energies of ions and ion− water clusters based on an accurate value for the absolute aqueous solvation free energy of the proton, J. Phys. Chem. B. 110 (32) (2006) 16066–16081, https://doi.org/10.1021/jp063552y.
[34] V. Graziani, A. Marrone, N. Re, C. Coletti, J.A. Platts, A. Casini, A multi-level theoretical study to disclose the binding mechanisms of gold (III)–bipyridyl compounds as selective aquaglyceroporin inhibitors, Chemistry–A European Journal 23 (55) (2017) 13802–13813, https://doi.org/10.1002/chem.201703092.
[35] S.J. Leach, H.A. Scheraga, Effect of light scattering on ultraviolet difference spectra1, J. Am. Chem. Soc. 82 (18) (1960) 4790–4792, https://doi.org/10.1021/ja01503a008.
[36] M.J. Frisch, G.W. Trucks, H.B. Schlegel, G.E. Scuseria, M.A. Robb, J.R. Cheeseman, G. Scalmani, V. Barone, G.A. Petersson, H. Nakatsuji, et al., Gaussian 16, Revision C.01, Gaussian, Inc., Wallingford CT, 2016.
[37] J.D. Chai, M. Head-Gordon, Systematic optimization of long-range corrected hybrid density functionals, J. Chem. Phys. 128 (8) (2008) 084106, https://doi.org/10.1063/1.2834918.
[38] K.A. Peterson, D. Figgen, E. Goll, H. Stoll, M. Dolg, Systematically convergent basis sets with relativistic pseudopotentials. II. Small-core pseudopotentials and correlation consistent basis sets for the post-d group 16–18 elements, J. Chem. Phys. 119 (21) (2003) 11113–11123, https://doi.org/10.1063/1.1622924.
[39] F. Weigend, R. Ahlrichs, Balanced basis sets of split valence, triple zeta valence and quadruple zeta valence quality for H to Rn: design and assessment of accuracy, Phys. Chem. Chem. Phys. 7 (18) (2005) 3297–3305, https://doi.org/10.1039/B508541A.
[40] C.J. Cramer, Essentials of Computational Chemistry: Theories and Models, John Wiley & Sons, 2013.
[41] I. Tolbatov, N. Re, C. Coletti, A. Marrone, An insight on the gold (I) affinity of golB protein via multilevel computational approaches, Inorg. Chem. 58 (16) (2019) 11091–11099, https://doi.org/10.1021/acs.inorgchem.9b01604.
[42] G. Sciortino, J.D. Maréchal, E. Garribba, Integrated experimental/computational approaches to characterize the systems formed by vanadium with proteins and enzymes, Inorg. Chem. Front. 8 (8) (2021) 1951–1974, https://doi.org/10.1039/D0QI01507E.
[43] I. Tolbatov, N. Re, C. Coletti, A. Marrone, Determinants of the lead (II) affinity in pbrR protein: a computational study, Inorg. Chem. 59 (1) (2019) 790–800, https://doi.org/10.1021/acs.inorgchem.9b03059.
[44] R. Paciotti, I. Tolbatov, V. Graziani, A. Marrone, N. Re, C. Coletti, Insights on the activity of platinum-based anticancer complexes through computational methods, in: AIP Conference Proceedings vol. 2040, AIP publishing, 2018, November, https://doi.org/10.1063/1.5079061 no. 1.
[45] S. Todisco, M. Latronico, V. Gallo, N. Re, A. Marrone, I. Tolbatov, P. Mastrorilli, Double addition of phenylacetylene onto the mixed bridge phosphinito–phosphanido Pt (I) complex [(PHCy$_2$)Pt(μ-PCy$_2$){κ^{2}P,O-μ-P(O)Cy$_2$}Pt(PHCy$_2$)](Pt–Pt), Dalton Trans. 49 (20) (2020) 6776–6789, https://doi.org/10.1039/D0DT00923G.
[46] I. Tolbatov, A. Marrone, C. Coletti, N. Re, Computational studies of au (I) and au (III) anticancer metallodrugs: a survey, Molecules 26 (24) (2021) 7600, https://doi.org/10.3390/molecules26247600.
[47] I. Tolbatov, A. Marrone, Reactivity of N-heterocyclic carbene half-sandwich Ru-, Os-, Rh-, and Ir-based complexes with cysteine and selenocysteine: a computational study, Inorg. Chem. 61 (1) (2021) 746–754, https://doi.org/10.1021/acs.inorgchem.1c03608.
[48] I. Tolbatov, A. Marrone, Kinetics of reactions of dirhodium and diruthenium paddlewheel tetraacetate complexes with nucleophilic protein sites: computational insights, Inorg. Chem. 61 (41) (2022) 16421–16429, https://doi.org/10.1021/acs.inorgchem.2c02516.
[49] I. Tolbatov, A. Marrone, Reaction of dirhodium and diruthenium paddlewheel tetraacetate complexes with nucleophilic protein sites: a computational study, Inorg. Chim. Acta 530 (2022) 120684, https://doi.org/10.1016/j.ica.2021.120684.
[50] J. Tomasi, B. Mennucci, E. Cancès, The IEF version of the PCM solvation method: an overview of a new method addressed to study molecular solutes at the QM ab initio level, J. Mol. Struct. (THEOCHEM) 464 (1–3) (1999) 211–226, https://doi.org/10.1016/S0166-1280(98)00553-3.

[51] A. Klamt, C. Moya, J. Palomar, A comprehensive comparison of the IEFPCM and SS (V) PE continuum solvation methods with the COSMO approach, J. Chem. Theory Comput. 11 (9) (2015) 4220–4225, https://doi.org/10.1021/acs.jctc.5b00601.
[52] J.D. Chai, M. Head-Gordon, Long-range corrected hybrid density functionals with damped atom–atom dispersion corrections, Phys. Chem. Chem. Phys. 10 (44) (2008) 6615–6620, https://doi.org/10.1039/B810189B.
[53] Y. Zhao, D.G. Truhlar, The M06 suite of density functionals for main group thermochemistry, thermochemical kinetics, noncovalent interactions, excited states, and transition elements: two new functionals and systematic testing of four M06-class functionals and 12 other functionals, Theor. Chem. Accounts 120 (1) (2008) 215–241, https://doi.org/10.1007/s00214-007-0310-x.
[54] J.P. Perdew, K. Burke, M. Ernzerhof, Generalized gradient approximation made simple, Phys. Rev. Lett. 77 (18) (1996) 3865, https://doi.org/10.1103/PhysRevLett.77.3865.
[55] A.D. Becke, Density-functional exchange-energy approximation with correct asymptotic behavior, Phys. Rev. A 38 (6) (1988) 3098, https://doi.org/10.1103/PhysRevA.38.3098.
[56] J.P. Perdew, Density-functional approximation for the correlation energy of the inhomogeneous electron gas, Physical Review B 33 (12) (1986) 8822, https://doi.org/10.1103/PhysRevB.33.8822.
[57] J.P. Perdew, in: P. Ziesche, H. Eschrig (Eds.), Electronic Structure of Solids '91, Akademie Verlag, Berlin, 1991, p. 11.
[58] Y. Zhao, D.G. Truhlar, A new local density functional for main-group thermochemistry, transition metal bonding, thermochemical kinetics, and noncovalent interactions, J. Chem. Phys. 125 (19) (2006) 194101, https://doi.org/10.1063/1.2370993.
[59] S. Grimme, J. Antony, S. Ehrlich, H. Krieg, A consistent and accurate ab initio parametrization of density functional dispersion correction (DFT-D) for the 94 elements H-Pu, J. Chem. Phys. 132 (15) (2010) 154104, https://doi.org/10.1063/1.3382344.
[60] V. Barone, M. Cossi, Quantum calculation of molecular energies and energy gradients in solution by a conductor solvent model, Chem. A Eur. J. 102 (11) (1998) 1995–2001, https://doi.org/10.1021/jp9716997.
[61] A.V. Marenich, C.J. Cramer, D.G. Truhlar, Universal solvation model based on solute electron density and on a continuum model of the solvent defined by the bulk dielectric constant and atomic surface tensions, J. Phys. Chem. B. 113 (18) (2009) 6378–6396, https://doi.org/10.1021/jp810292n.
[62] A.D. Becke, Density functional thermochemistry. III. The role of exact exchange, J. Chem. Phys. 98 (7) (1993) 5648–5652, https://doi.org/10.1063/1.464913.
[63] C. Lee, W. Yang, R.G. Parr, Development of the Colle-Salvetti correlation-energy formula into a functional of the electron density, Phys. Rev. B 37 (2) (1988) 785, https://doi.org/10.1103/PhysRevB.37.785.
[64] W.R. Wadt, P.J. Hay, Ab initio effective core potentials for molecular calculations. Potentials for main group elements Na to bi, J. Chem. Phys. 82 (1) (1985) 284–298, https://doi.org/10.1063/1.448800.
[65] A. Albeck, H. Weitman, B. Sredni, M. Albeck, Tellurium compounds: selective inhibition of cysteine proteases and model reaction with thiols, Inorg. Chem. 37 (8) (1998) 1704–1712, https://doi.org/10.1021/ic971456t.